Supplement of Biogeosciences, 23, 1223–1243, 2026
https://doi.org/10.5194/bg-23-1223-2026-supplement
© Author(s) 2026. CC BY 4.0 License.

Biogeosciences Open Access EGU

Supplement of

Satellite-derived Ecosystem Functional Types capture ecosystem functional heterogeneity at regional scale

Beatriz P. Cazorla et al.

Correspondence to: Beatriz P. Cazorla (b.cazorla@ugr.es)

The copyright of individual parts of the supplement might differ from the article licence.

Supplementary material

S1. Remote sensing data source selection

In this study, we choose MODIS data instead of other satellites with higher spatial resolution (e.g. Landsat or Sentinel-2) because MODIS has several advantages in terms of data availability and quality (e.g. more years of data and cloud-free image every 16-days). Since the MODIS sensor provides a daily image of the Earth, such high frequency (1 per day) increases the probability of finding a cloud-free image every 16-days. MODIS provides the best composite value every 16 days (i.e. chooses the best available pixel value from all the acquisitions from the 16 day period), applying an algorithm that selects the image atmospherically corrected bi-directional surface reflectances and select the image with lowest cloud presence, the lowest view angle, and the highest EVI value. Although Landsat has a lower pixel size, their images have a lower frequency (i.e., 1 image every 16 days). Thus, the fixed acquisition schedule makes it less probable to acquire good-quality imagery for a particular place periodically (especially if clouds occur frequently over the area of interest, e.g. winter dates).

Landsat product with the largest time series is Landsat 7 (1999-actually) however, on May 31, 2003, the satellite's scan-line corrector failed. The scan-line corrector is a device on the satellite that keeps the scan lines parallel to each other. Without the Scan Line Corrector (SLC), the scan lines are mis-aligned and there are wedge-shaped data gaps in the images. Providers offer different procedures for filling-in the data gaps, but each amounts to using data from good images prior to 2003 to do so. Obviously the further one gets from 2003, the less valid this approach will be. Therefore, since 2003 SLC failure of Landsat 7, Landsat 8 is the only fully operational Landsat satellite in orbita, but covers a shorter time series than MODIS (Landsat8 covers from 2013 to actually, while MODIS covers from 2001 to actually).

Other satellites have also been considered for their use, as Sentinel-2, which also has a higher spatial resolution but the time series is still too short for our study (2015-present). Therefore, the period of Sentinel-2 data is not covered by FLUXNET data, i.e. Sentinel-2 starts taking data in 2015 and the available FLUXNET database goes up to this year.

S2. EFT class thresholds for EVI_mean, EVI_SD, and EVI_DMAX

Table S1. Interannual quartile thresholds derived from the 14-year EVI time series used as class breaks for EVI_mean and EVI_SD, and seasonal thresholds used for EVI_DMAX. For EVI_DMAX, the four intervals agree with the four seasons of the year. For EVI_mean and EVI_sSD, we extracted the first, second, and third quartiles for each year and then calculated the interannual mean of each quartile (their average over the 14-year period).

Ecosystem functional attribute	EFT character code	Range
EVI mean (productivity)	A	0 - 0. 277
	B	0. 277 - 0. 325
	C	0. 325 - 0.366
	D	> 0.366
EVI SD (seasonality)	a	> 0.115
	b	0.094 - 0.115
	c	0.062 - 0.094
	d	0 - 0.062
EVI DMAX (phenology)	1	Spring
	2	Summer
	3	Autumn
	4	Winter

S3. Schematic table of EFT codes combinations and their ecological meaning

Table S2. Examples of EFT code combinations and their ecological interpretation. Capital letters denote quartile-based classes of annual mean EVI (EVI_mean; proxy for productivity), lowercase letters indicate quartile-based classes of seasonal EVI variability (EVI_SD; proxy for the seasonality of carbon gains), and numbers correspond to the season in which the maximum EVI (DMAX) occurs (1 = spring, 2 = summer, 3 = autumn, 4 = winter). Representative PFT associated with each EFT are provided to illustrate the ecological meaning of the classification.

EFT code	EVI_mean (A–D)	Productivity level	EVI_SD (a–d)	Seasonality level	DMAX	Season of max EVI	Example PFTs (from EC sites in this study)
Da1	D	High productivity	a	High seasonality	1	Spring	Deciduous broadleaf and mixed forests (e.g., DE-Lnf, FR-Fon, IT-Col, DK-Sor)
Ad1	A	Low productivity	d	Low seasonality	1	Spring	Mediterranean shrublands (e.g., ES-LJu, IT-Noe)
Ba1	B	Moderate–low productivity	a	High seasonality	1	Spring	Croplands and wetlands (e.g., DE-Geb, DE-Kli, BE-Lon, CZ-wet)
Cb1	C	Moderate–high productivity	b	Moderately high seasonality	1	Spring	Croplands (e.g., CH-Oe1, DE-Seh, DE-RuS)
Ac2	A	Low productivity	c	Moderate–low seasonality	2	Summer	Alpine evergreen needleleaf forests (e.g., CH-Dav)

Ab2	A	Low productivity	b	Moderately high seasonality	2	Summer	High-altitude evergreen needleleaf forests (e.g., DE-Lkb)
Cc1	C	Moderate–high productivity	c	Moderate–low seasonality	1	Spring	Mixed forests (e.g., BE-Bra, CZ-BK1)
Cd1	C	Moderate–high productivity	d	Low seasonality	1	Spring	Mediterranean pine forests (e.g., FR-Pue)
Db4	D	High productivity	b	Moderately high seasonality	4	Winter	Mediterranean croplands with winter maximum (e.g., IT-BCi)
Ad4	A	Low productivity	d	Low seasonality	4	Winter	Arid shrublands (e.g., ES-Amo) — low assimilation, carbon source except in winter
Aa1	A	Very low productivity	a	Very high seasonality	1	Spring	Alpine grasslands (e.g., IT-MBo, IT-Tor)
Da2	D	High productivity	a	High seasonality	2	Summer	Mountain grasslands (e.g., AT-Neu, CH-Fru, DE-Gri)

S4. EC-EFT Discriminant Analysis

During the comparison of the performance of PFTs and EFTs to discriminate the seasonal dynamics of NEE, we took into account the unbalanced sample size due to the different number of classes of EFTs (20) and PFTs (7) represented by FLUXNET2015 and the different number of EC sites per PFT class (which ranged between 3 and 31). To do this we performed the following steps:

First, we calculated all possible combinations (C) without repetitions between the 18 EFT and the 7 PFT classes (C(18,7) = 31834). Second, we discarded all combinations that had different numbers of EC sites in the EFT and PFT classes being combined. Third, for each combination, we applied discriminant analysis to assess how well the EFT classification and the PFT classification performed to discriminate the seasonal dynamics of NEE. For each discriminant analysis, we obtained five metrics of performance (Table S2). Fourth, to assess whether there existed significant differences in the performance metrics between EFTs and PFTs, we applied the Wilcoxon non-parametric test. For each combination of the number of classes and the number of EC sites, there was a different number of discriminant analyses in the EFT subset and in the PFT subset (Table S1). To account for such an unbalanced design during the Wilcoxon test, we fixed the sample size to the smaller subset (either from the EFT or the PFT classification) and randomly bootstrapped the performance metrics from the bigger one. Fifth, we calculated the mean and standard deviation of each metric obtained by the EFTs and PFTs classifications, the average p-value, and the percentage of times that we obtained significant differences (p-value <0.05) between EFTs and PFTs.

To assess whether different satellite-derived EFT classes correspond to different NEE dynamics and whether sites under the same EFT exhibit similar NEE dynamics, we applied discriminant analysis. We selected the EFT of the MODIS pixel where each EC site was located and its corresponding interannual average of the seasonal cycle of NEE for the available years. EC sites' fluxes were regarded as the ground truth against which the satellite data were compared to calculate five performance metrics: Kappa, Accuracy, Precision, Recall, and F1 score (Table S2).

Table S3. Number of discriminant analysis (i.e. combinations) for each number of classes and number of EC sites in the EFT and in the PFT subsets.

		n classes EFTs						n classes PFTs					
		2	**3**	**4**	**5**	**6**	**7**	**2**	**3**	**4**	**5**	**6**	**7**
n EC sites	**3**	32						6					
	4	38	56					3	3				
	5	24	112					2	6				
	6	26	160	392				5	2	3			
	7	12	160	536				3	7	2			
	8		160	585	1078				9	3	1		
	9	10	126	592				1	3	9			
	10		96	520	1640				2	7	3		
	11	4	82	464	1668			4	3	2	5		
	12	1	60	373	1655	3504		6	21	6	2	1	
	13		50	320	1466	3868			2	3	3	1	
	14		28	238	1312				6	61	6		
	15		27	196	1112	3676			51	2	1	3	
	16		12	136	922	3396			6	41	6	2	
	17		8	100	746		7252		9	72	4		1
	18		2	54	590	2597			2	4	6	2	
	19			28	428					81	21		
	20			12	267	1817				11	16	61	
	21			4	160	1332				5	7	1	
	22			1	78	945	4153			4	21	4	2
	23				36	580	3308				13	91	2
	24				10	337					5	7	
	25				4	154	1610				12	4	7
	26					70	958					6	5
	27					20						8	
	28					6	232					4	4
	29						90						2
	30						25						3
	31						4						7

Table S4. Contingency table (in %) of EFTs and PFTs. The numbers show the percentage of EFTs classified in each PFT. EFTs are coded as follows: capital letters correspond to the EVI annual mean (EVI_mean) level, ranging from A to D for low to high productivity. Small letters show the seasonal standard deviation (EVI_SD), ranging from a to d for high to low seasonality of carbon gains. The numbers indicate the season when the maximum EVI took place (DMAX): (1) spring, (2) summer, (3) autumn, (4) winter.

%	Cropland	Deciduous broadleaf trees	Evergreen needleleaf trees	Grassland	Mixed trees	Shrubland	Wetland
Aa1				29	12		
Ab2			10				
Ac1			20				
Ac2			10				
Ad1						67	
Ad4					12	33	
Ba1	27						100
Bc1			20				
Bd1	13				25		
Bd2			10		13		
Ca1	7						
Cb1	33						
Cc1	7		10		13		
Cd1	7				25		
Cd3			10				
Da1		100					
Da2				57			
Db1				14			
Db4	6						
Dd1			10				

S5. Supplementary Figures

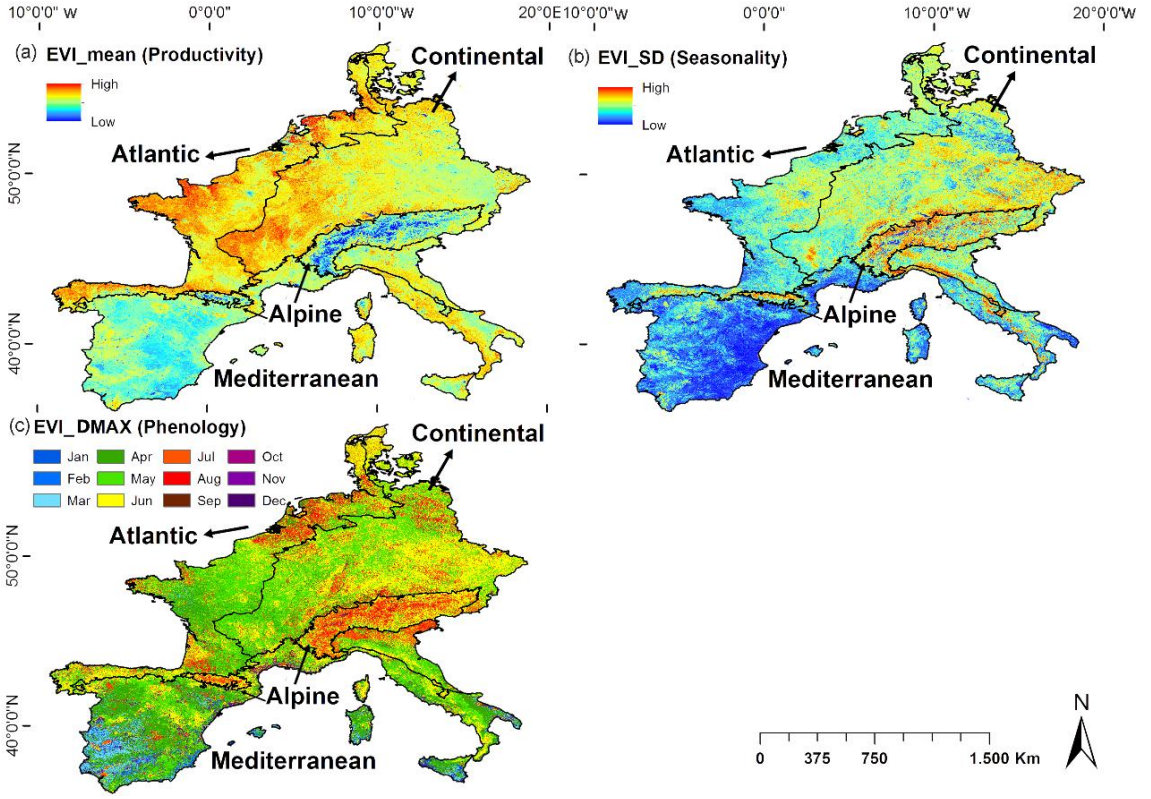

Fig. S1. Ecosystem Functional Attributes based on the 2001-2014 time-series of satellite images of the Enhanced Vegetation Index (EVI) captured by the MODIS-Terra sensor (MOD13Q1.C006 product): (a) EVI annual mean (EVI_mean; an estimator of annual primary production); (b) the EVI seasonal standard deviation (EVI_SD; a descriptor of seasonality); and (c) the date of maximum EVI (EVI_DMAX; an indicator of phenology). Biogeographical regions are based on the official European biogeographical regions map (EEA, 2016).

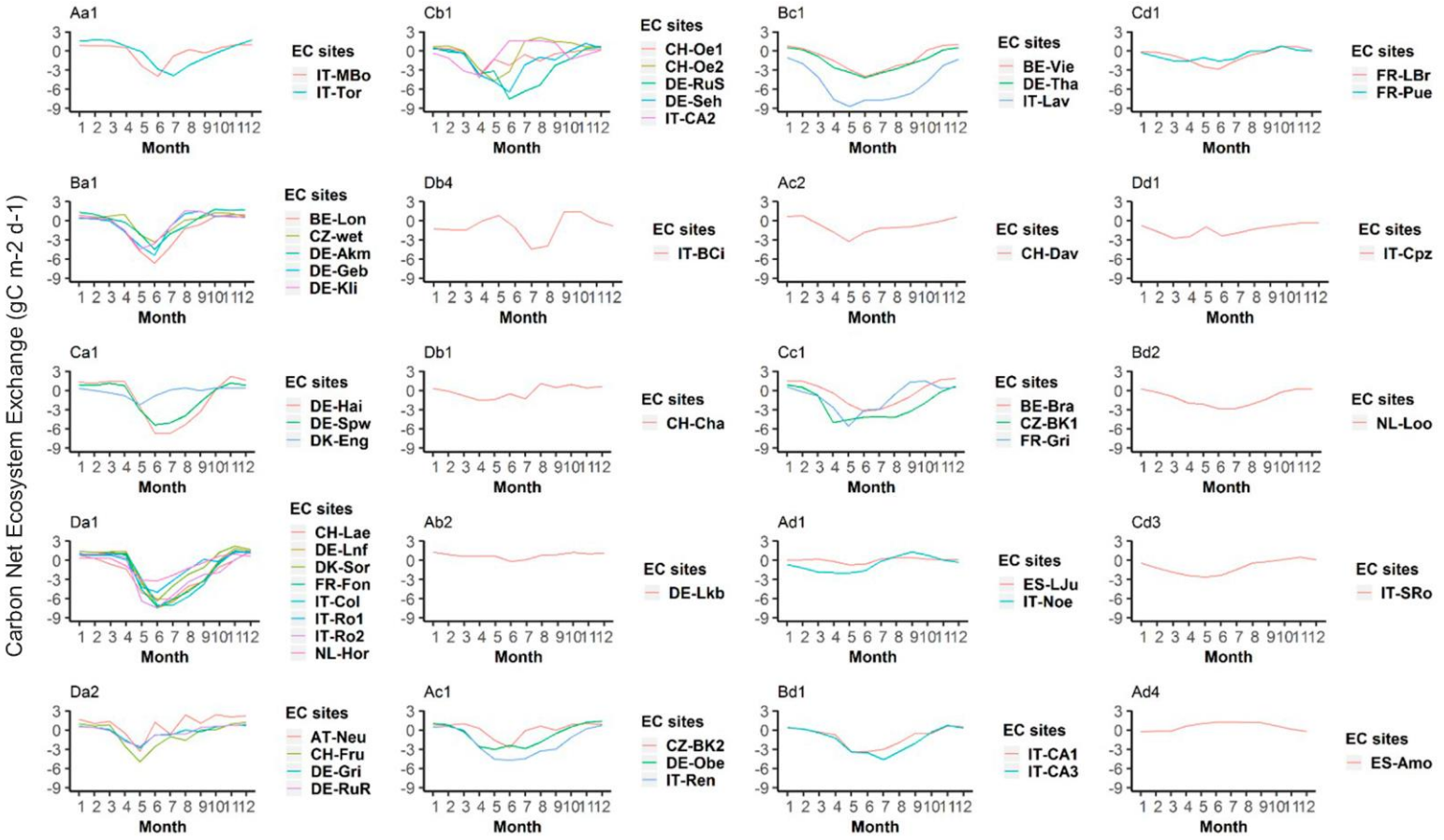

Fig. S2. Variability inter EFTs: annual mean of NEE dynamics from different EC places with the same EFT.

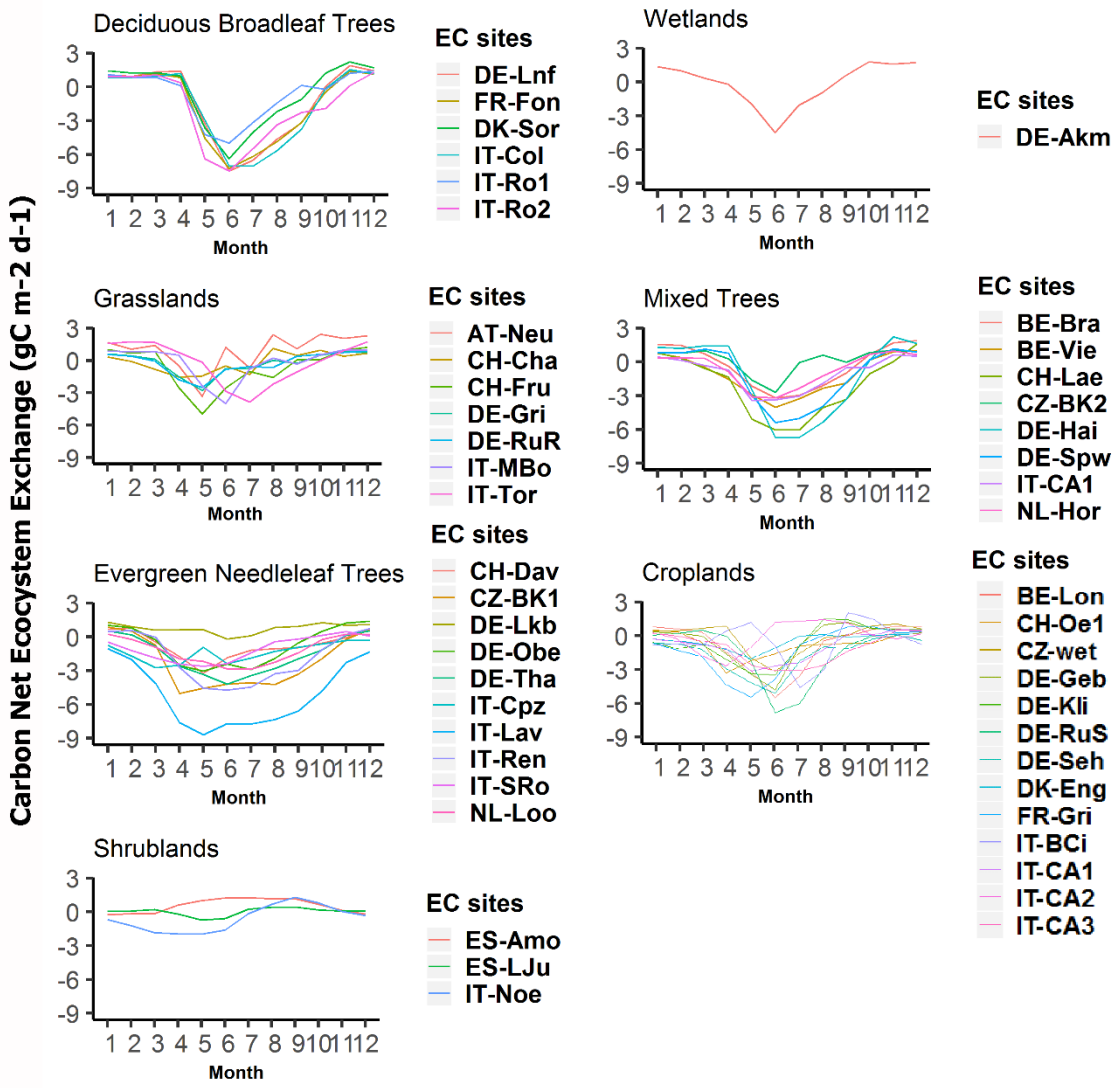

Fig. S3. Variability inter PFTs and intra EFTs: Annual mean of NEE dynamics from different places with the same PFT and different EFT.

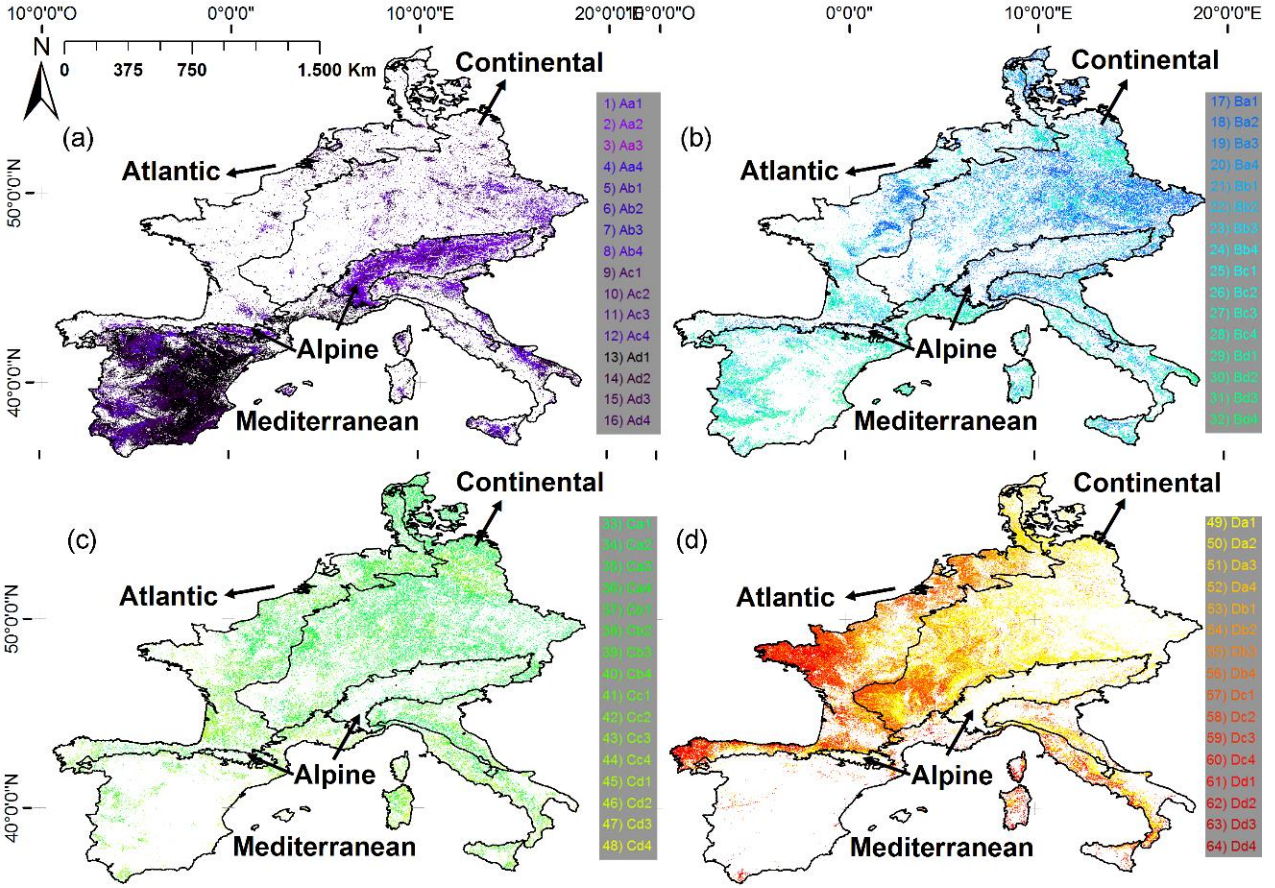

Fig. S4. Ecosystem Functional Types (EFTs) productivity maps based on the 2001-2014 time-series of satellite images of the Enhanced Vegetation Index (EVI) captured by the MODIS-Terra sensor (MOD13Q1.C006 product): (a) EFTs with low productivity (category A) (b) EFTs with low-medium productivity (category B); (c) EFTs with medium-high productivity (category C); and (d) EFTs with high productivity (category D). Biogeographical regions are based on the official European biogeographical regions map (EEA, 2016).

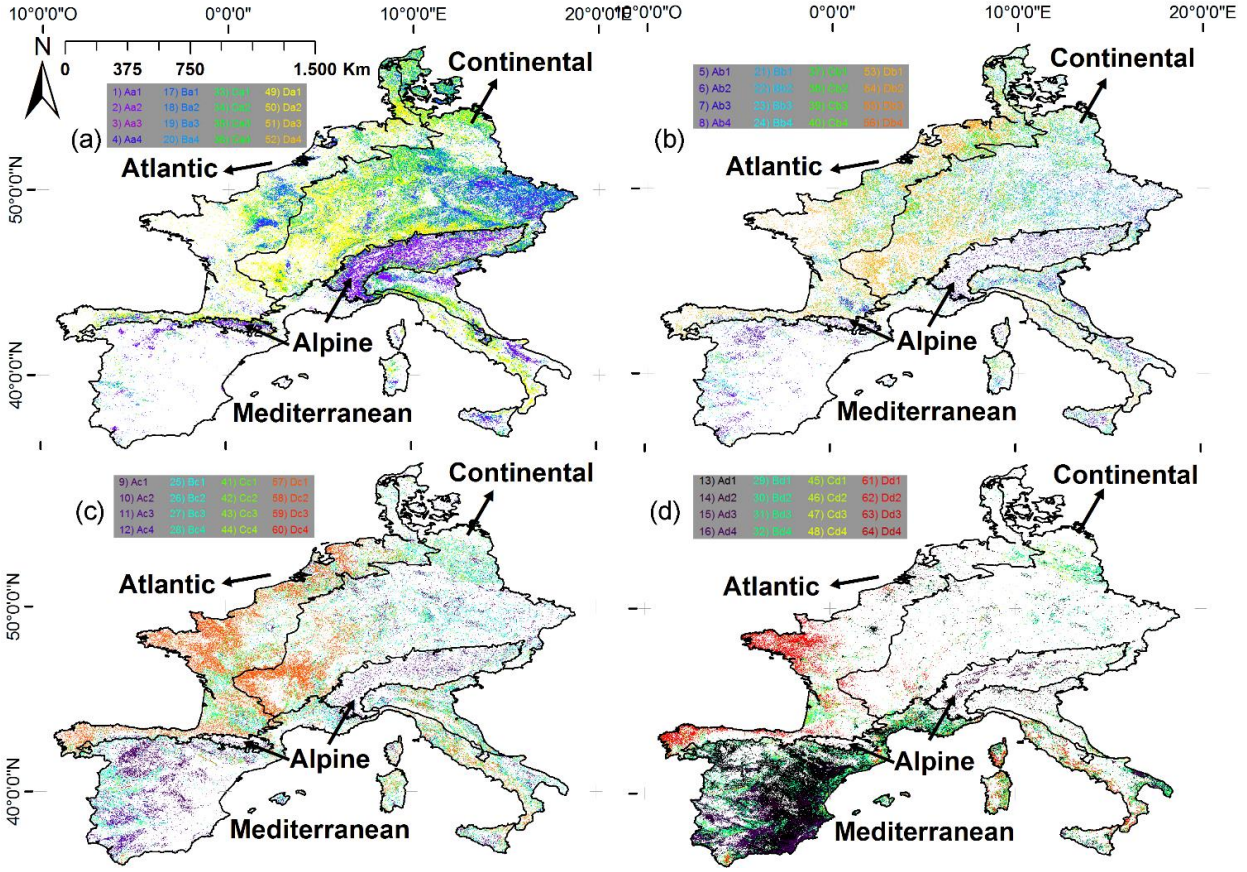

Fig. S5. Ecosystem Functional Types (EFTs) seasonality maps based on the 2001-2014 time-series of satellite images of the Enhanced Vegetation Index (EVI) captured by the MODIS-Terra sensor (MOD13Q1.C006 product): (a) EFTs with high seasonality (category a) (b) EFTs with high-medium seasonality (category b); (c) EFTs with medium-low seasonality (category c); and (d) EFTs with low seasonality (category d). Biogeographical regions are based on the official European biogeographical regions map (EEA, 2016).

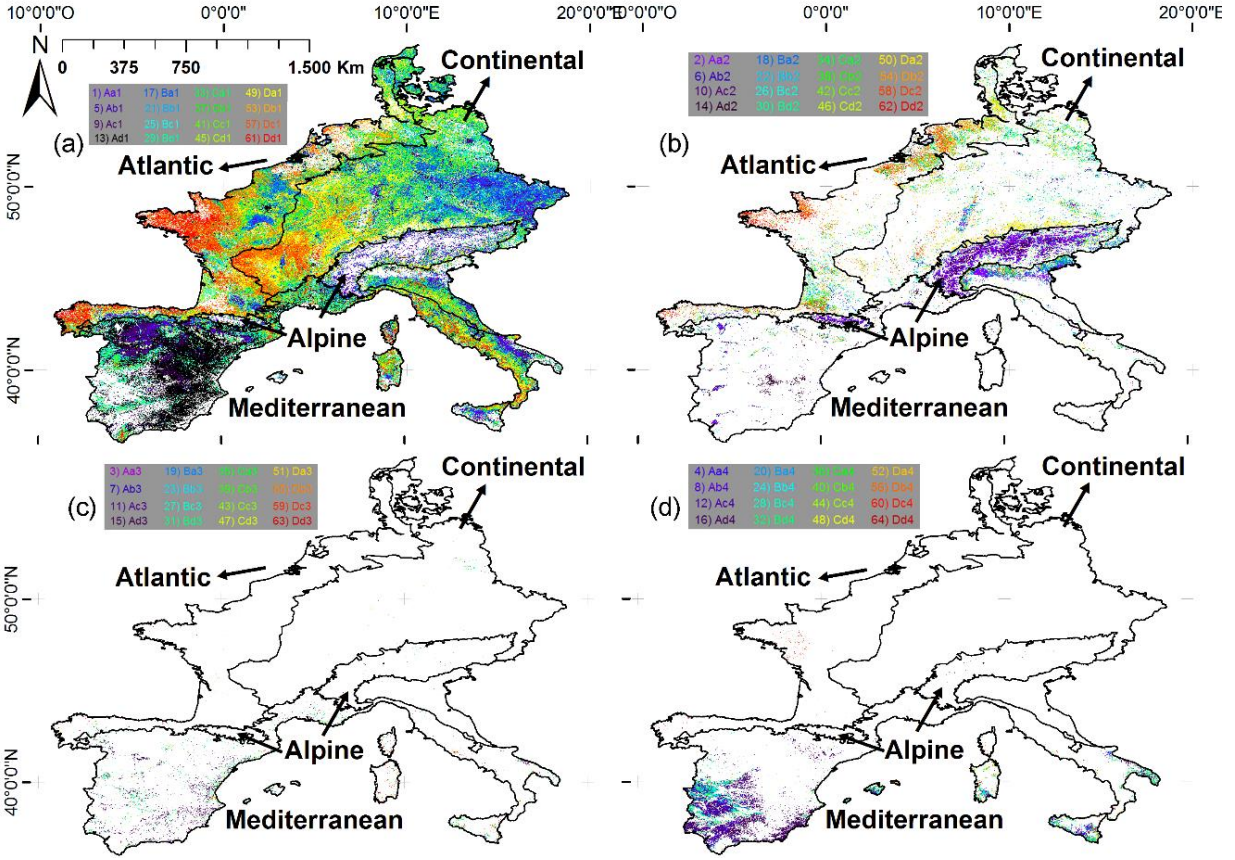

Fig. S6. Ecosystem Functional Types (EFTs) phenology maps based on the 2001-2014 time-series of satellite images of the Enhanced Vegetation Index (EVI) captured by the MODIS-Terra sensor (MOD13Q1.C006 product): (a) EFTs with spring phenology (category 1) (b) EFTs with summer phenology (category 2); (c) EFTs with autumn (category 3); and (d) EFTs with winter phenology (category 4). Biogeographical regions are based on the official European biogeographical regions map (EEA, 2016).

S6. EFT clustering and functional characterization

The EFT-clustered map (Fig. S7) depicts the spatial distribution of 16 ecosystem functional clusters across Europe, derived from MODIS EVI time series (2001–2014). The clusters were obtained by aggregating 64 EFTs according to three functional attributes: annual mean productivity, intra-annual seasonality, and month of maximum greenness. Each cluster therefore represents a group of ecosystems with similar temporal dynamics of vegetation functioning. Clear large-scale patterns emerge. Northern Europe is dominated by clusters with low productivity and strong seasonality, reflecting short, cold growing seasons. Central Europe exhibits more homogeneous clusters with high and stable productivity. Southern Europe, especially the Iberian Peninsula, shows a fine-scale mosaic of clusters characterized by early spring peaks and strong summer constraints. Mountain regions such as the Alps and Pyrenees form distinct clusters with late phenological peaks and high seasonality. Together, the clusters summarize the major bioclimatic and phenological gradients of Europe, providing a functional classification useful for ecological assessment and climate-change studies.

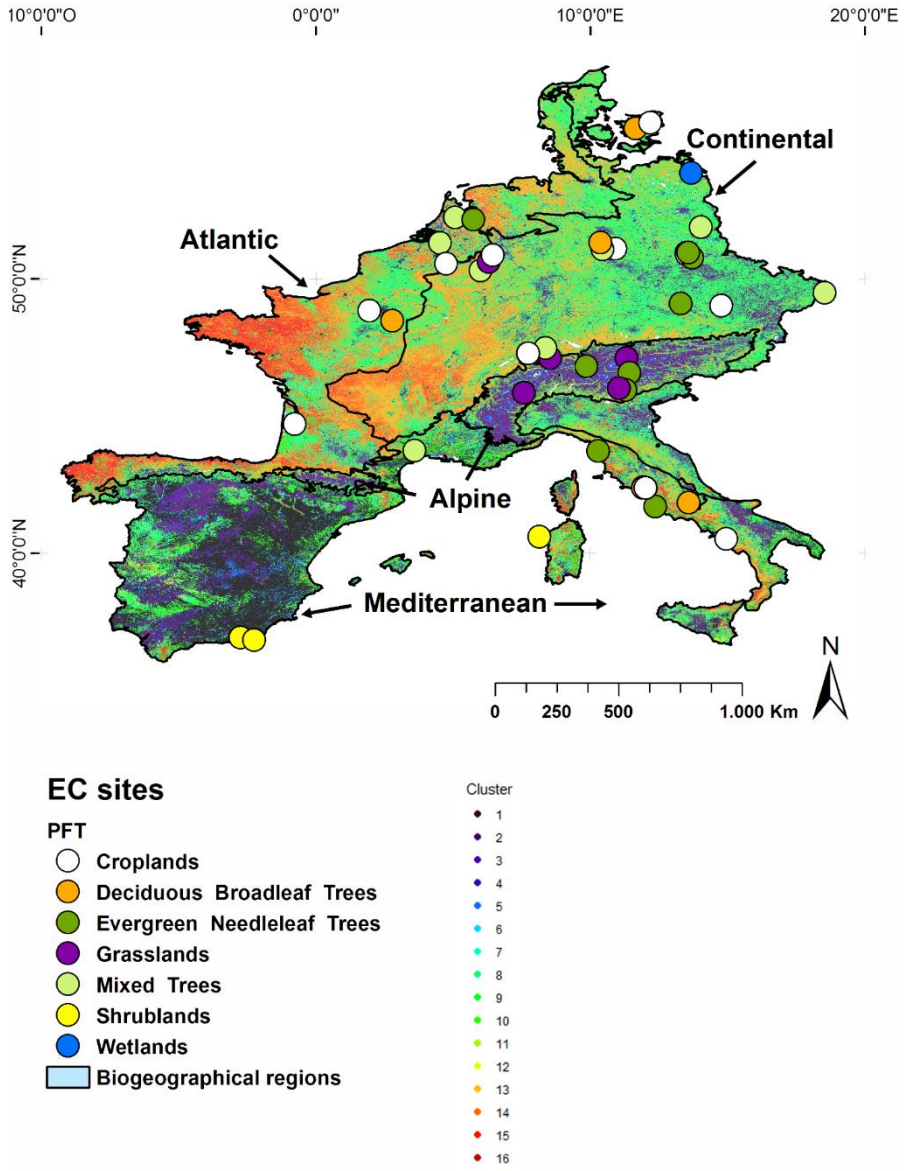
10°0'0"O
0°0'0"
10°0'0"E
20°0'0"E
50°0'0"N
40°0'0"N
Continental
Atlantic
Alpine
Mediterranean
N
0
250
500
1.000 Km
EC sites
PFT
Croplands
Deciduous Broadleaf Trees
Evergreen Needleleaf Trees
Grasslands
Mixed Trees
Shrublands
Wetlands
Biogeographical regions
Cluster
1
2
3
4
5
6
7
8
9
10
11
12
13
14
15
16

Fig. S7. Spatial distribution of Ecosystem Functional Types (EFTs) across Europe, grouped into 16 functional clusters (background colours). Circles indicate the locations of eddy-covariance (EC) sites, coloured according to their plant functional type (PFT: croplands, deciduous broadleaf trees, evergreen needleleaf trees, grasslands, mixed forests, shrublands, and wetlands). Grey outlines denote the main European biogeographical regions (Atlantic, Continental, Alpine, and Mediterranean).

The optimal number of functional clusters was determined using the Elbow Method (Fig. S8), which assesses how the total within-cluster sum of squares (WSS) decreases as the number of clusters (k) increases. As shown in Supplementary Figure S8, WSS drops sharply for small values of k, indicating that additional clusters substantially improve cluster compactness. However, the rate of decrease progressively slows, and the curve begins to flatten between approximately k = 10 and k = 20, marking the onset of diminishing returns. Based on this stabilization region, we selected k = 16, which provides an effective balance between reducing within-cluster variance and avoiding unnecessary over-partitioning. Choosing 16 clusters retains meaningful functional differentiation while preserving ecological interpretability.

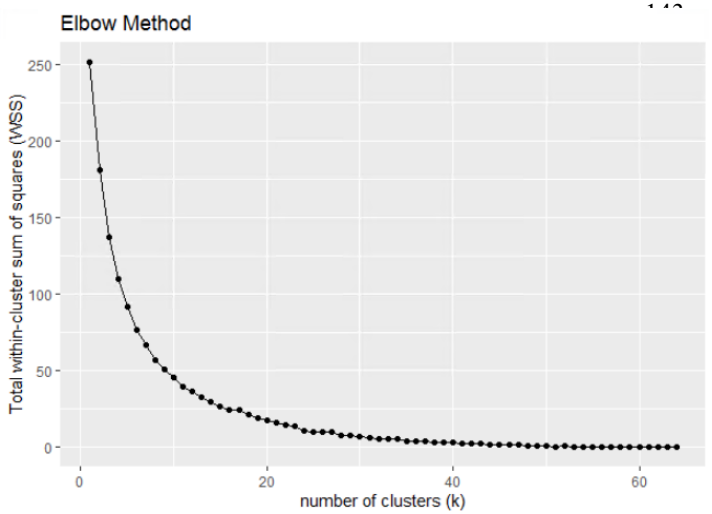

Fig. S8. The plot shows the total within-cluster sum of squares (WSS) as a function of the number of clusters (k). The WSS decreases sharply for small k values, indicating substantial gains in cluster compactness.

The figure S9 shows a non-metric multidimensional scaling (NMDS) ordination of the 64 EFTs derived from MODIS EVI time series. Each EFT is represented by a point labelled with its alphanumeric code (A–D × a–d × 1–4), which reflects combinations of productivity level, seasonality, and phenological timing. The ordination is based on three Ecosystem Functional Attributes (EFAs): annual mean productivity, intra-annual variability, and month of maximum greenness. EFTs are coloured according to the 16 functional clusters identified through k-means clustering. The NMDS clearly separates groups of EFTs with similar functional behaviour, revealing coherent clusters that reflect gradients in productivity (A→D), phenological patterns, and seasonal amplitude. Proximity of points indicates functional similarity, whereas distinct clusters represent contrasting ecosystem functioning. This ordination thus provides a functional summary of relationships among the 64 EFTs and illustrates the rationale for aggregating them into 16 ecologically interpretable clusters.

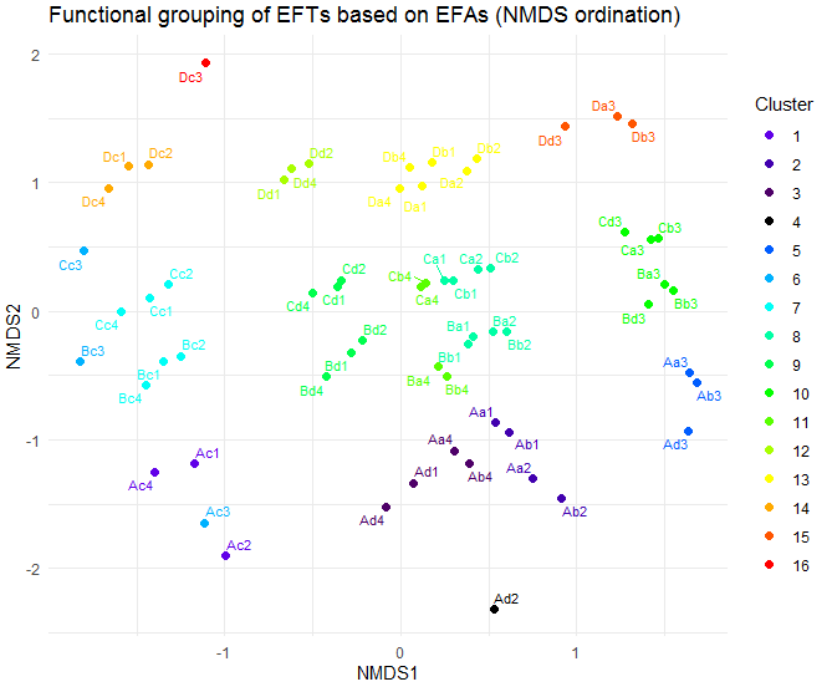

Figure S9. Non-metric multidimensional scaling (NMDS) ordination of the 64 EFTs coloured by their corresponding functional clusters.

The figure S10 shows the stressplot of the non-metric multidimensional scaling (NMDS). The high non-

metric $R^2 = 0.96$ indicates that the NMDS solution preserves the rank order of dissimilarities well, meaning that ecosystems that are functionally similar in the original EFA space remain close in the ordination. The linear $R^2 = 0.789$ shows a reasonably strong, though not perfect, linear correspondence between original and ordination distances, as expected in non-metric techniques. The tight alignment of points around the monotonic fit and the steep lower section of the curve confirm that the NMDS configuration provides a high-quality and reliable representation of the functional dissimilarities among EFTs.

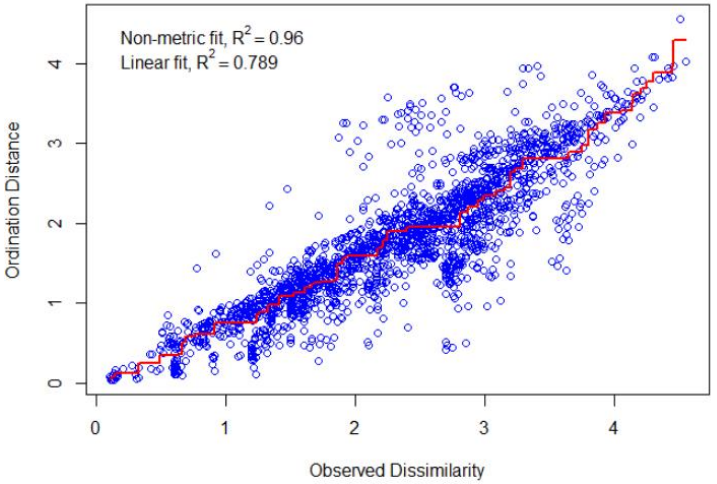

Figure S10. Stressplot of the non-metric multidimensional scaling (NMDS). Blue points represent the relationship between observed dissimilarities and NMDS ordination distances, while the red stepped line shows the monotonic regression fitted by the NMDS algorithm.

Figure S11 shows boxplots of the three EVI-derived metrics used to characterize EFTs across the 16 EFT clusters ordered by productivity. The clusters, represented consistently by their functional colour palette, exhibit clear gradients in ecosystem functioning. Mean EVI (Mean_mean) increases progressively from clusters 1 to 11, reflecting a transition from low-productivity to high-productivity vegetation types, while the most productive clusters (12–16) show distinctly higher values. The intra-annual variability (SD_mean) also varies markedly across clusters, with some low-productivity groups showing high variability (e.g., cluster 1) and mid-productivity clusters exhibiting comparatively low seasonal amplitude (e.g., clusters 8–11). The timing of maximum greenness (DMax_mode)

reveals functional distinctions in seasonal dynamics, with early peaks in low-productivity clusters, mid-season peaks in intermediate clusters, and late peaks in several high-productivity clusters. Together, these distributions highlight the functional coherence and ecological differentiation of the 16 EFT clusters, confirming that the productivity-ordered classification captures meaningful gradients in both magnitude and seasonality of vegetation functioning across Europe.

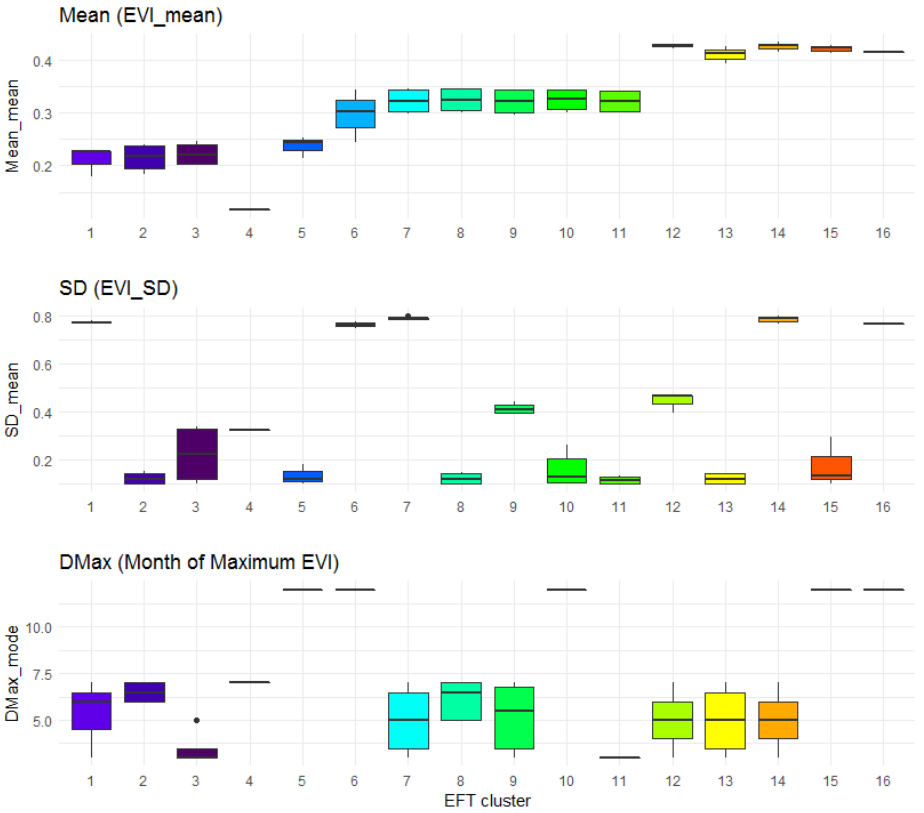

Fig. S11. Boxplots of functional metrics for the 16 productivity-ordered EFT clusters. Panels show the distribution of (a) Mean EVI (Mean_mean), (b) seasonal variability of EVI (SD_mean), and (c) month of maximum EVI (DMax_mode). Colours correspond to the EFT cluster palette used throughout the study. The figure illustrates clear gradients in vegetation productivity and seasonality across EFTs, confirming the ecological distinctiveness of the 16 clusters.